JACS
JOURNAL OF THE AMERICAN CHEMICAL SOCIETY
Article
pubs.acs.org/JACS

Fluorogenic α-Tocopherol Analogue for Monitoring the Antioxidant Status within the Inner Mitochondrial Membrane of Live Cells

Katerina Krumova, Lana E. Greene, and Gonzalo Cosa*

Department of Chemistry and Center for Self-Assembled Chemical Structures (CSACS-CRMAA), McGill University, 801 Sherbrooke Street West, Montreal, Quebec H3A 0B8, Canada

Supporting Information

ABSTRACT: We report here the preparation of a lipophilic fluorogenic antioxidant (Mito-Bodipy-TOH) that targets the inner mitochondrial lipid membrane (IMM) and is sensitive to the presence of lipid peroxyl radicals, effective chain carriers in the lipid chain autoxidation. Mito-Bodipy-TOH enables monitoring of the antioxidant status, i.e., the antioxidant load and ability to prevent lipid chain autoxidation, within the inner mitochondrial membrane of live cells. The new probe consists of 3 segments: a receptor, a reporter, and a mitochondria-targeting element, constructed, respectively, from an α-tocopherol-like chromanol moiety, a BODIPY fluorophore, and a triphenylphosphonium cation (TPP). The chromanol moiety ensures reactivity akin to that of α-tocopherol, the most potent naturally occurring lipid soluble antioxidant, while the BODIPY fluorophore and TPP ensure partitioning within the inner mitochondrial membrane. Mechanistic studies conducted either in homogeneous solution or in liposomes and in the presence of free radical initiators show that the antioxidant activity of Mito-Bodipy-TOH is on par with that of α-tocopherol. Studies conducted on live fibroblast cells further show the antioxidant depletion in the presence of methyl viologen (paraquat), a known agent of oxidative stress and source of superoxide radical anion (and indirectly, a causative of lipid peroxidation) within the mitochondria matrix. We recorded a ca. 8-fold emission enhancement with Mito-Bodipy-TOH in cells stressed with methyl viologen, whereas no enhancement was observed in control studies with untreated cells. Our findings underscore the potential of the new fluorogenic antioxidant Mito-Bodipy-TOH to study the chemical link between antioxidant load, lipid peroxidation and mitochondrial physiology.

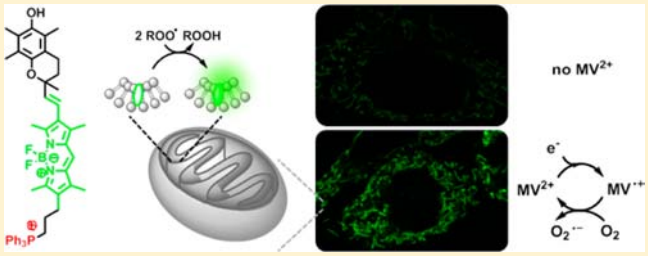

INTRODUCTION

The inner mitochondrial membrane is a major site of generation of reactive oxygen species (ROS) produced as byproducts of the mitochondrial electron transport chain. Polyunsaturated fatty acids (PUFA) within the inner mitochondrial membrane are particularly vulnerable to ROS elicited oxidative damage.[1] PUFA residues may readily undergo autoxidation, a chain reaction initiated by a ROS such as the hydroxyl radical and next propagated by lipid peroxyl radicals, effective chain carriers in the lipid chain autoxidation which are themselves ROS.[2−4] Reactions of peroxyl radicals are slow compared to the time scale of most other free radical reactions and thus the peroxyl radical is the dominant species present in the chain.[4] Importantly, the action of antioxidants such as α-tocopherol (TOH), an effective lipid peroxyl radical scavenger and the most active naturally occurring lipid soluble antioxidant,[2] inhibits lipid chain autoxidation.[5]

The deleterious effect of ROS in the mitochondrial membrane, protein, and DNA has been implicated in the onset of multiple pathologies associated with mitochondrial dysfunction.[6−9] There is a complex relationship between mitochondrial ROS-mediated damage and a range of neurodegenerative disorders[10,11] including Parkinson's disease,[12−14] Alzheimer's disease,[1,15] amyotropic lateral sclerosis (ALS),[16] and ataxia.[17]

Noninvasive imaging methodologies that enable real-time monitoring of the generation, accumulation, and consumption of ROS within the mitochondria of live cells are of paramount importance to unravel the chemical mechanism behind the cellular pathologies associated to ROS. Significant progress has been accomplished in this direction in the last 5 years exploiting fluorescence imaging with fluorogenic probes that preferentially target mitochondria and that react specifically with H_2O_2,[18,19] superoxide,[20] and highly reactive ROS.[21,22] Recently, Murphy and co-workers developed a membrane embedded ratiometric fluorescent sensor (MitoPerOx) that is susceptible to lipid peroxyl radicals by tagging the fluorescent probe C11-BODIPY$^{581/591}$ with a mitochondria-targeting moiety.[23] This probe contains a BODIPY core conjugated via a dienyl link to a phenyl group. Reaction with peroxyl radicals leads to cleavage of the dienyl link to give a chromophore with reduced conjugation characterized by a blue-shifted emission.[24]

Our own interest lies in determining the antioxidant status within the inner mitochondrial lipid membrane, i.e., the ability

Received: August 8, 2013
Published: October 10, 2013

   dx.doi.org/10.1021/ja408227f | J. Am. Chem. Soc. 2013, 135, 17135−17143

of the mitochondria to prevent lipid chain autoxidation. A probe is thus required capable of reporting via, e.g., emission enhancement of the depletion of α-tocopherol in the inner mitochondrial membrane and the onset of the lipid chain autoxidation. Here we describe the preparation, characterization, and application to live cell imaging of a lipophilic fluorogenic α-tocopherol analogue probe Mito-Bodipy-TOH. The new probe was designed to both mimic the structure and reactivity of α-tocopherol[25−29] and to target the inner mitochondrial membrane. The photophysical, reactivity, and live cell studies conducted position Mito-Bodipy-TOH as a versatile tool to study the relationship between antioxidant content, ROS elicited oxidative damage, mitochondrial physiology, and mitochondrial dysfunction.

RESULTS AND DISCUSSION

Design of Mitochondria-Targeting Fluorogenic Antioxidant. The new probe consists of 3 segments: a receptor, a reporter, and a mitochondria-targeting element (Figure 1). A

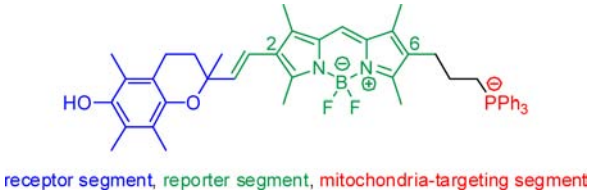

Figure 1. Structure of mitochondria-targeting fluorogenic antioxidant (Mito-Bodipy-TOH). The three segments are colored to facilitate visualization.

chromanol ring bearing the chemical structure of the most potent naturally occurring free radical scavenger α-tocopherol[2] was chosen as a receptor. This choice ensured a high specificity toward lipid peroxyl radicals, effective chain carriers and the dominant ROS species encountered in lipid membranes under oxidative stress. Importantly, it further warranted a rapid rate of reaction of the probe with lipid peroxyl radicals, on par with that of α-tocopherol (vide infra), characterized by a rate constant of 3×10^6 M^{-1} s^{-1} in homogeneous solution.[2]

We used a BODIPY fluorophore as the reporter segment. BODIPY fluorophores have optimal spectroscopic properties and they are lipophilic. Further, BODIPY structures are amenable to synthetic modifications to introduce chemical groups and to tune their redox potentials.[25−27] BODIPY dyes are thus easily tunable to afford exergonic photoinduced electron transfer (PeT) from the receptor (chromanol) moiety.[25,30] An intramolecular switch based on PeT may thus render the probe nonemissive. Oxidation of the receptor upon reaction with peroxyl radicals deactivates PeT and emission in the reporter segment is restored.[25,26,28,29] Our strategy renders a fluorogenic probe that upon scavenging two peroxyl radicals (with the concomitant oxidation of the receptor segment) undergoes a fluorescence enhancement. Reporting is thus directly related to peroxyl radical scavenging.[25−29] A vinyl linker connecting the chromanol moiety to the BODIPY core helps minimize the distance between the receptor and reporter segments, further favoring PeT and providing a lipophilic substrate.

We utilized a largely delocalized positively charged segment for preferential accumulation of the probe in the inner mitochondrial membrane.[31−33] We resorted to the use of phosphonium groups, established by Murphy[23,34−37] and subsequently utilized by others[18,19,38−44] to selectively direct attached cargo (e.g., fluorescent probes) to the mitochondrial matrix. The third segment of the probe thus contained a triphenylphosphonium cation (TPP) appended via an alkyl tail to the BODIPY dye. The alkyl group additionally increases the lipophilic character of the fluorogenic probe, facilitating its insertion into the mitochondrial membrane.

Synthesis of Mitochondria-Targeting Fluorogenic Antioxidant. Asymmetric BODIPY dyes are traditionally prepared by condensation of an α-formyl pyrrole and a pyrrole with a free α-position.[45] We rationalized that synthetically it would be most feasible to first prepare a chromanol-α-formyl pyrrole adduct (segment A, Scheme 1). Heck coupling was

Scheme 1. (A) Retrosynthetic Analysis of the Mitochondria-Targeting Fluorogenic Probe; (B) Structures of Fluorogenic Probes 1 (Nontargeting) and 2 (Targeting) and Fluorescent Controls 3 (Nontargeting) and 4 (Targeting)

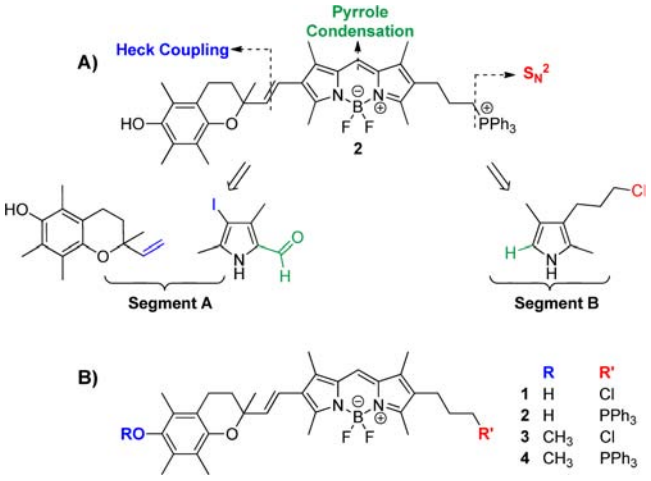

employed to couple both units via a vinyl linker. We subsequently assembled the asymmetric BODIPY dye. Here we envisioned that the pyrrole with a free α-position should have a functional group to enable the installation of the TPP moiety. The desired nucleophilic pyrrole was thus prepared bearing a propyl chloride group (segment B, Scheme 1). Condensation between the chromanol-α-formyl pyrrole and segment B was then carried out to obtain the chromanol-BODIPY precursor **1** (Scheme 1). Mito-Bodipy-TOH **2** was next obtained upon the nucleophilic substitution of the chloride in **1** with triphenylphosphine to install the positively charged phosphonium tag. Control compounds **3** and **4** were subsequently prepared bearing a methoxy group on the chromanol ring.

To accomplish the Heck coupling, we first prepared the chromanol alkene **6** and the iodo-formyl pyrrole **7** utilizing previously reported procedures (Scheme 2).[29,46,47] We further protected the pyrrole with a methoxymethyl (MOM) group to yield compound **8**. Traditional protecting groups used for pyrroles such as tert-butyloxycarbonyl (Boc) and benzoyl (Bz) groups were not amenable to our synthetic conditions as they were easily deprotected under the high temperatures (100 °C) required for of the Heck reaction (Scheme 2).

We subsequently proceeded with the Heck coupling of compounds **6** and **8**. Standard Heck coupling conditions involving triethylamine and $Pd(OAc)_2$ in dimethylformamide (DMF) at 100 °C led exclusively to deiodination of pyrrole **8**.

dx.doi.org/10.1021/ja408227f | J. Am. Chem. Soc. 2013, 135, 17135−17143

Scheme 2. Synthesis of Segment A

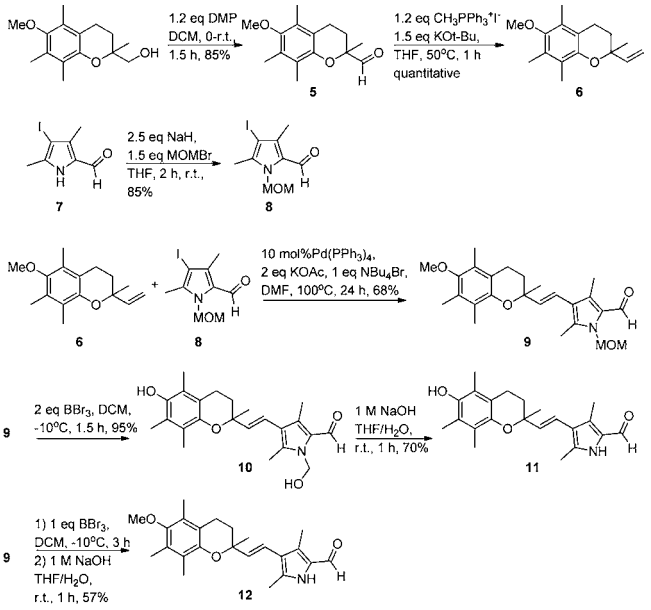

Examining the mechanism of the reaction we concluded that the loss of iodine was possibly due to the base used. We modified the conditions employing potassium acetate, tetrabutylammonium bromide, and 10% $Pd(PPh_3)_4$ (Scheme 2).[48] The reaction was heated to 100 °C for 24 h. The coupling yielded the desired chromanol-pyrrole adduct **9** in 68% yield. Deiodination was still observed but only in 30% yield.

To subject compound **9** to a condensation with the pyrrole bearing a free α-position to form the BODIPY fluorophore, a removal of both protecting groups (MOM on the pyrrole and methoxy on the chromanol) was necessary. MOM deprotection proved to be challenging as most of the product decomposed under the acidic conditions used (1 M HCl or 1 M trifluoroacetic acid). Only 10% yield was achieved under these conditions. We thus developed an alternative two-step deprotection approach (Scheme 2). In the first step, addition of 2 equiv of BBr_3 at −10 °C removed both the methoxy group on the phenol and the methoxy part of the MOM protection to yield **10**. Compound **10** is a hemiaminal, which was hydrolyzed to formaldehyde and fully deprotected pyrrole **11** following treatment with 1 M NaOH.[49] Maintaining the right temperature throughout the reaction of the formation of **10** was crucial. An increase in the temperature led to decomposition of the intermediate **10**.

We next proceeded with the preparation of the pyrrole with a free α-position (segment B). The synthesis of compound **17** was accomplished following previously developed procedures (Scheme 3).[50,51]

Scheme 3. Synthesis of Segment B

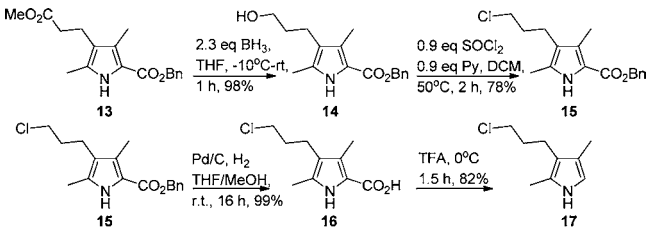

Having prepared all the necessary segments to assemble the BODIPY precursor, we proceeded with their condensation. Pyrrole **17** was subjected to a condensation reaction with pyrrole **11** in the presence of phosphorus oxychloride (Scheme 4). Complexation of the so formed dipyrromethene with BF_3·OEt and diisopropylethylamine yielded the chormanol-BODIPY adduct **1**.

Scheme 4. Synthesis of Mitochondria-Targeting Fluorogenic Probe Mito-Bodipy-TOH (2) and Its Precursor 1

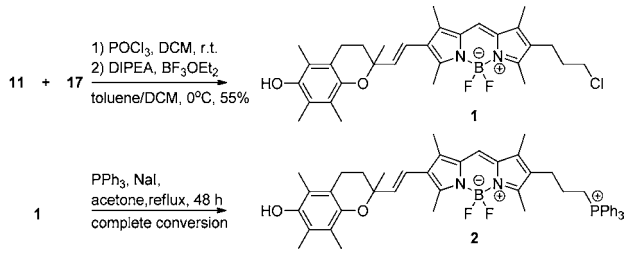

The final step in the synthesis of the new mitochondria-targeting fluorogenic antioxidant **2** was the nucleophilic substitution of the chloride in the lipophilic tail of the BODIPY dye with triphenylphosphene to install the positively charged phosphonium tag (Scheme 4). The substitution was facilitated by the use of sodium iodide.

Control compounds **3** and **4** were next prepared bearing the methoxy group on the chromanol ring (Scheme 5). Starting

Scheme 5. Synthesis of Fluorescent Mitochondria-Targeting Control Compound 4 and Its Precursor 3

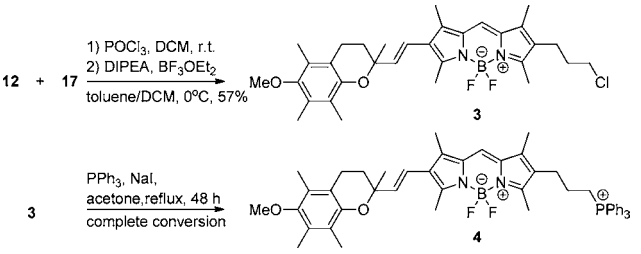

from compound **9**, it was partially deprotected using 1 equiv of BBr_3, where only the pyrrole protecting MOM-group was removed to yield compound **12**. The same synthetic procedures described above and outlined in Scheme 5 were next employed to obtain **3** and **4**.

Spectroscopic Properties of the Fluorogenic Antioxidant and Analogues. Table 1 lists the absorption and emission maxima, emission quantum yields, and absorption extinction coefficients determined in acetonitrile for compounds **1**−**4** (see also Figure 2). Compounds **1** and **2** displayed

Table 1. Photophysical Properties of Dyes 1−4 in Acetonitrile at Room Temperature[a]

	Abs λ_{max} (nm)	Em λ_{max} (nm)	Φ_f	$\varepsilon \times 10^3$ (M^{-1} cm^{-1})
1	536	582	0.04	34
2	537	572	0.02	34
3	536	585	0.30	34
4	536	582	0.23	34

[a]Quantum yields were measured using PM605 in acetonitrile as a standard (Φ_{st} = 0.72).[30]

dx.doi.org/10.1021/ja408227f | J. Am. Chem. Soc. 2013, 135, 17135−17143

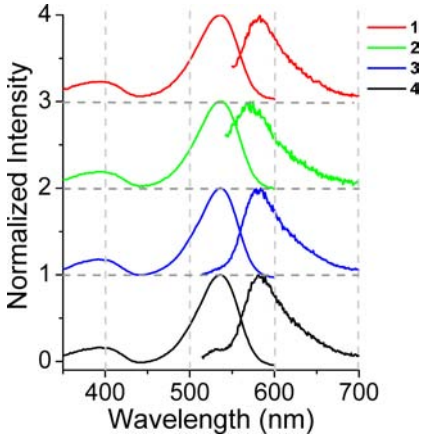

Figure 2. Normalized absorption and emission spectra obtained in acetonitrile for compounds **1**–**4**. Plots are offset with respect to each other in the ordinate axis to facilitate comparison.

an emission quantum yield 10-fold lower than that of counterparts **3** and **4** that bear a methoxy-protected phenol. Whereas the former two compounds can readily undergo intramolecular PeT from the chromanol moiety to the BODIPY fluorophore,[25,26,29] the introduction of the methoxy group in **3** and **4** increases the oxidation potential of the chromane moiety deactivating the intramolecular PeT. Emissive compounds **3** and **4** thus provide for exquisite controls in cell studies with fluorogenic compounds **1** (lipophilic yet not organelle-specific) and **2** (mitochondria-targeting), respectively (vide infra).

Peroxyl Radical Scavenging Activity of Mito-Bodipy-TOH. To investigate the sensitivity and reactivity of **1** and **2** toward peroxyl radicals in homogeneous (acetonitrile solution) and microheterogeneous media (liposome suspension), these fluorogenic antioxidants were subjected to reaction with peroxyl radicals generated via thermolysis of azo-initiators in oxygen equilibrated solutions. The analysis of the intensity-time trajectories we recorded provided a measure of the sensitivity (fluorescence enhancement) and reactivity/antioxidant activity of the new probes when experiments were conducted with competing antioxidants. The experimental procedures and analysis used have been previously reported by us.[25,29] Three different azo-initiators, two generating lipophilic peroxyl radicals (AMBN and MeO-AMVN)) and one a hydrophilic peroxyl radical (ABAP), were used to examine the reactivity and sensitivity of the probes (Figure S1).

A significant, ca. 10-fold, fluorescence enhancement was recorded with time following reaction of **1** and **2** with peroxyl radicals generated from AMBN in homogeneous media. The enhancement is consistent with the deactivation of the intramolecular PeT process upon oxidation of the receptor segment, and provides a magnitude for the sensitivity of the new probe toward ROS.

The reactivity of **1** and **2** toward peroxyl radicals was determined in competitive kinetic studies performed in the presence of either α-tocopherol or 2,2,5,7,8-pentamethyl-6-hydroxychroman (PMHC), an α-tocopherol analogue lacking the phytyl chain (Figure 3).[29] Briefly, the new probe was used as a signal carrier in competitive kinetic studies in the presence of TOH and PMHC. In our assay, we used a microplate reader to monitor over time the emission intensity enhancement of membrane-embedded Mito-Bodipy-TOH upon scavenging peroxyl radicals when alone or in the presence of competing

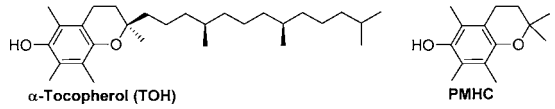

Figure 3. Structures of α-tocopherol and PMHC.

antioxidants. The relative antioxidant activities of the antioxidants were obtained from the analysis of the initial slope of a plot of $\ln[(I_\infty - I_t)/(I_\infty - I_o)]$ vs $\ln[1 - t/\tau]$. Studies in acetonitrile show that peroxyl radicals react with the same rate constant with **1**, **2**, TOH and PMHC compounds (Table S1). The inherent chemical reactivity of the chromanol ring in **1** and **2** is thus on par with the reactivity of α-tocopherol and PMHC and is not diminished by its coupling to the BODIPY segment or the presence of the TPP segment (Figure S2A in the Supporting Information section and discussion therein). The absolute value for the rate constant of reaction of the new probe with peroxyl radicals may thus be positioned in the order of ca. 3×10^3 M^{-1} s^{-1}, the value reported for α-tocopherol under similar conditions.[52,53]

Control experiments were further conducted with the fluorescent analogue **3** in the presence of the competing antioxidant PMHC (Figure S2B). No emission enhancement was observed for compound **3**, where PeT is not operational, and where the methoxy protected phenol cannot undergo H-abstraction by peroxyl radicals (Figure S2B). A linear drop in emission intensity with time was recorded once PMHC is consumed (Figure S2B). This result is consistent with the onset of radical-mediated BODIPY degradation.

A 6-fold increase in fluorescence intensity with time was observed for **1** or **2** when embedded in Egg PC lipid membranes upon exposure to hydrophilic (ABAP source) or lipophilic (MeO-AMVN) peroxyl radicals. Competitive kinetic studies conducted on liposome suspensions show that Mito-Bodipy-TOH and α-tocopherol have the same rate constant for reaction with peroxyl radicals. In stark contrast, PMHC outcompetes the new probes for reaction with peroxyl radicals (Figure S4 and discussion therein). Mobility and to a lesser extent physical accessibility account for the larger relative antioxidant activity of tocopherol analogues bearing short (PMHC) over long (α-tocopherol) aliphatic tails, but that otherwise have the same inherent chemical reactivity.[29,54] Importantly, our competing kinetic studies not only pinpoint the similar antioxidant activity of α-tocopherol and Mito-Bodipy-TOH, but further underscore that Mito-Bodipy-TOH is embedded within the membrane much like α-tocopherol.

Monitoring Antioxidant Load in the Mitochondria of Living Cells. We initially conducted fluorescence colocalization studies to ensure that the probe localizes in mitochondria. Studies were conducted involving either the fluorogenic probe Mito-Bodipy-TOH (**2**) or its mitochondria targeting (**4**) or nontargeting fluorescent analogue (**3**), and MitoTracker Deep Red (a commercially available mitochondrial indicator). As a model cell line we used NIH 3T3 mouse embryo fibroblast cells. Cells were simultaneously stained with a 1 μM solution of Mito-Bodipy-TOH and a 200 nM solution of MitoTracker Deep Red at 37 °C for 5 min. Upon selective excitation of Mito-Bodipy-TOH at 488 nm, the cells exhibited extremely faint, yet detectable, fluorescence (500–620 nm) in discrete subcellular locations as determined by confocal microscopy (Figure 4A1). Similar images were obtained upon selective excitation of MitoTracker Deep Red at 633 nm and emission collection from 650 to 740 nm (Figure 4A2). The

dx.doi.org/10.1021/ja408227f | J. Am. Chem. Soc. 2013, 135, 17135–17143

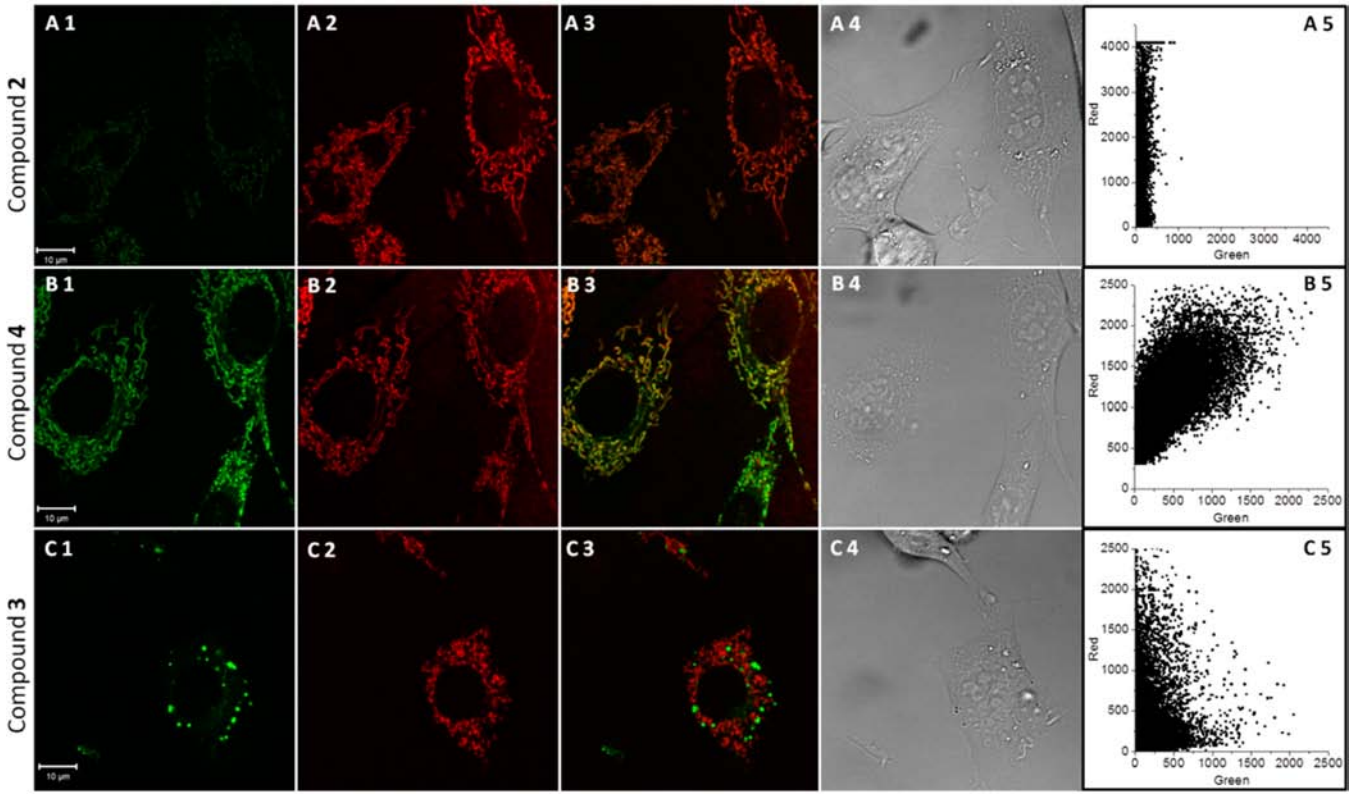

Figure 4. Confocal fluorescence images of live NIH 3T3 mouse embryo fibroblast cells acquired with 100× magnification objective. Cells were incubated with 1 μM probes **2**, **3**, and **4**, together with 200 nM MitoTracker Deep Red at 37 °C for 5 min in DMEM media supplemented with 10% FBS. Images display emission intensities collected in optical windows between 500 and 620 nm (for probes **2**, **3**, and **4**) upon excitation at 488 nm (125 μW laser power) and between 650 and 740 nm (for MitoTracker Deep Red) upon excitation at 633 nm (160 μW laser power): (A1) probe **2** (Mito-B-v-TOH); (A2) MitoTracker Deep Red; (A3) overlay of **1** and **2**; (A4) bright field image; (B1) probe **4**; (B2) MitoTracker Deep Red; (B3) overlay of **1** and **2**; (B4) bright field image; (C1) probe **3**; (C2) MitoTracker Deep Red; (C3) overlay of **1** and **2** (C4) bright field image. Cytofluorograms are displayed in panels A5−C5, demonstrating the extent of the colocalization for each probe (**2**, **3**, and **4**) with MitoTracker Deep Red. Scale bar is 10 μm.

colocalization of both dyes confirmed that Mito-Bodipy-TOH is localized in the mitochondria of live cells (Figure 4A3). We calculated the overlap coefficients for Mito-Bodipy-TOH and MitoTracker Deep Red according to Manders, a method that allows for reliable estimation of close proximity localization.[55] We obtained Manders' colocalization coefficients of M1 = 0.999 and M2 = 0.998, which further confirms the colocalization of the two molecules.

A 3D visualization of the cells enabled by stacks of confocal images further confirmed the colocalization of both dyes. A bright field image in turn revealed that cells are viable during the experiments (Figure 4A4). The fluorescent analogue **4** also showed colocalization with MitoTracker Deep Red under the same imaging conditions (Figure 4B1−4). We calculated Manders' colocalization coefficients of M1 = 0.984 and M2 = 0.723 for compound **4** and MitoTracker Deep Red. No colocalization was observed with MitoTracker Deep Red in control experiments using nontargeting fluorescent analogue **3** (Figure 4C1−4) with Mander's colocalization coefficients of M1 = 0.11 and M2 = 0.01. Taken together, these results establish that the lipophilic fluorogenic antioxidant Mito-Bodipy-TOH (**2**) and its fluorescent analogue **4** accumulate preferentially in the inner mitochondrial membrane due to the lipophilic cationic segment (phosphonium tag) and overall lipophilic moiety.

We next tested for the ability of Mito-Bodipy-TOH to report production of lipid peroxyl radicals and antioxidant depletion (scavenging of chromanol moieties) in live cell studies, see Figure 5. Methyl viologen (MV^{2+}) was used as a source of ROS in our experiments.[56,57] MV^{2+} is transported into mitochondria, where once in the matrix and in the presence of intracellular electron donors such as flavin-containing oxidoreductase enzymes,[58,59] it catalyzes the reduction of molecular oxygen to water yielding various ROS intermediates along the way. Specifically, MV^{2+} undergoes reduction to a radical cation that may be subsequently oxidized back to MV^{2+} upon reaction with molecular oxygen, yielding superoxide radical anion. A series of subsequent electron transfer and proton uptake reactions may lead to the formation of various intermediate ROS species such as hydrogen peroxide and hydroxyl radical[56] that ultimately lead to lipid chain autoxidation in the absence of antioxidants.

Fibroblast cells were cultured in media deprived of growth factors and supplemented with 1 mM MV^{2+} for 4 h. Following the removal of the MV^{2+} solution, the cells were incubated at 37 °C with 1 μM Mito-Bodipy-TOH in media. After 5 min, the cells were washed and the solution was replaced with media. Control cells were cultured in media with growth factors and no MV^{2+} under otherwise identical conditions. Both the healthy and stressed cells were imaged by confocal microscopy under the same imaging conditions (Figure 5). Whereas no emission enhancement was recorded in healthy cells (Figure 5A), we recorded a ca. 8-fold emission enhancement for Mito-Bodipy-TOH in stressed cells (Figure 5B). Clearly, the ongoing production of superoxide radial anion catalyzed by MV^{2+} within

dx.doi.org/10.1021/ja408227f | J. Am. Chem. Soc. 2013, 135, 17135−17143

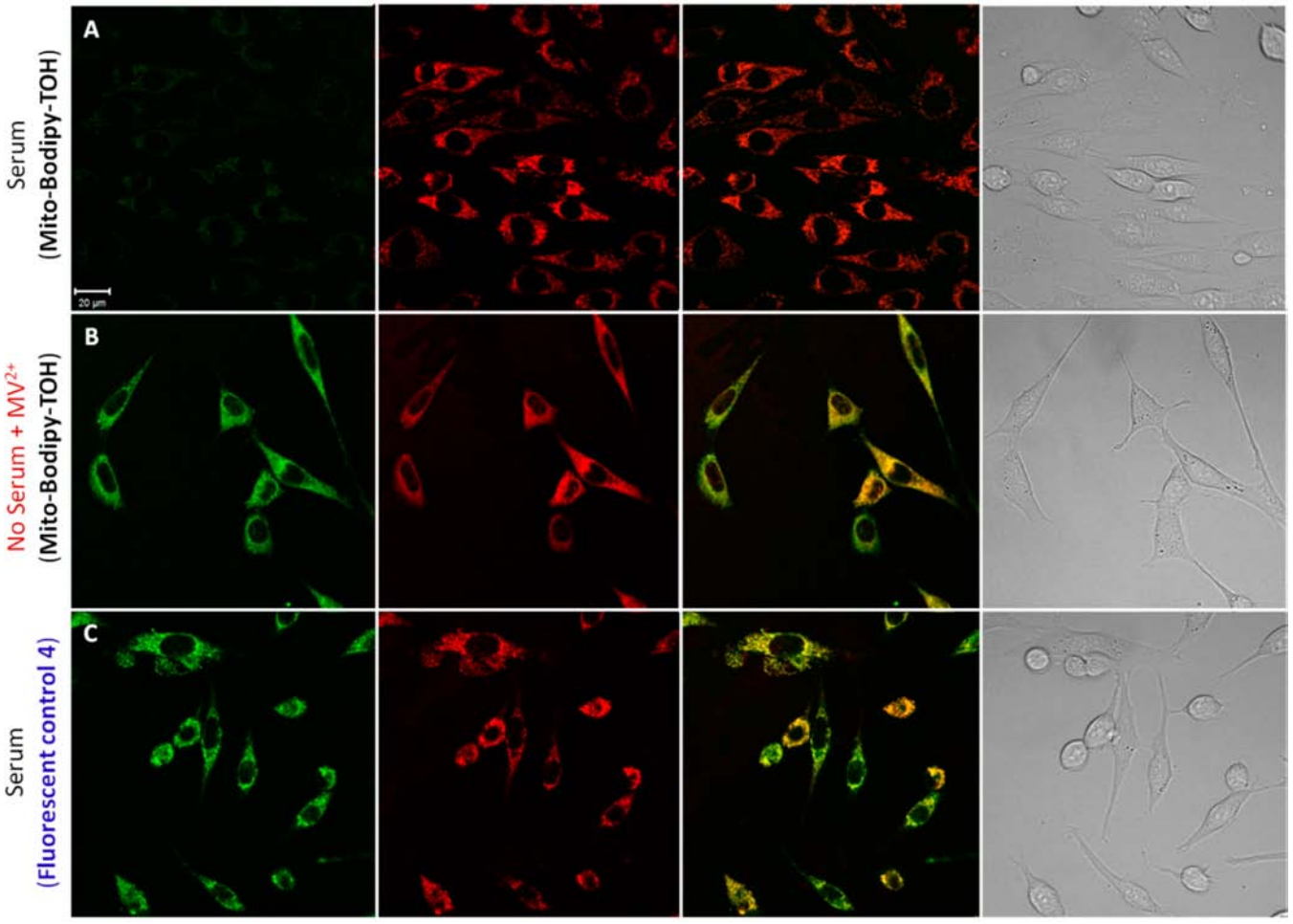

Figure 5. Detection of ROS with mitochondria-targeting fluorogenic probe Mito-Bodipy-TOH (**2**) in live NIH 3T3 mouse embryo fibroblast cells. Cells were incubated with 1 μM Mito-Bodipy-TOH and 200 nM MitoTracker Deep Red at 37 °C for 5 min. Emission intensities were recorded 15 min after incubation with the dyes and collected in optical windows between 500 and 620 nm (for probes **2** and **4**) upon excitation at 488 nm (125 μW laser power) and between 650 and 740 nm (for MitoTracker Deep Red) upon excitation at 633 nm (160 μW laser power). The panels show (left to right) confocal fluorescence images of 1 μM Mito-Bodipy-TOH, 200 nM MitoTracker Deep Red, overlay of the first two images, and bright field image of (A) fibroblast cells in the presence of 10% FBS, (B) fibroblast cells under oxidative stress conditions (deprived of growth factors and additionally stressed with 1 mM MV^{2+} for 4 h prior to imaging), (C) fibroblast cells in the presence of 10% FBS incubated with 1 μM control mitochondria-targeting fluorescent probe **4**. Scale bar is 20 μm.

the mitochondria matrix results in the production of lipid peroxyl radicals, among other ROS, which are readily scavenged by Mito-Bodipy-TOH, triggering its oxidation and concomitant emission enhancement.

The intensity recorded in control studies with fluorescent analogue **4** and healthy cells was ca. 7-fold higher than the one observed with the fluorogenic analogue Mito-Bodipy-TOH in healthy cells under otherwise identical conditions (Figure 5C), and similar to the intensity recorded for Mito-Bodipy-TOH in cells treated with MV^{2+}.

Altogether, our results confirm that the mitochondria-targeting fluorogenic antioxidant readily reports via emission enhancement the generation of lipid peroxyl radicals, and the depletion of antioxidants and thus the onset[25,26,29] of the lipid chain autoxidation in the inner mitochondrial membrane.

In closing, we note that Mito-Bodipy-TOH is complementary in its action to lipophilic probes such as MitoPerOx,[23] derived from C11-BODIPY581/591.[24] In the presence of peroxyl radicals, the former undergoes H-atom abstraction from its chromanol moiety with a rate constant comparable to that of α-tocopherol. Mito-Bodipy-TOH thus reports the antioxidant consumption, and the onset of lipid chain autoxidation.[60,61] In turn, C11-BODIPY581/591 and related probes rely on a slower reaction involving the breaking of the chromophore dienyl link upon reaction with lipid peroxyl radicals.[23,62] This reaction takes place once antioxidants have been consumed and lipid peroxyl radicals become the effective chain carriers in the lipid chain autoxidation.[63] Both probes thus target different stages of the membrane peroxidation process. Importantly, small concentrations of Mito-Bodipy-TOH should be employed in order to avoid changes in the antioxidant status of the live cell. The preferential accumulation of the fluorogenic antioxidant within the mitochondria might otherwise result in an enhanced protection of the mitochondrial function from oxidative damage.[36,37]

We also note that the intensity discrimination between the probe and its oxidized form may be exploited toward developing a ratiometric analysis based on fluorescence lifetimes. We are currently exploring experiments conducted in a fluorescence lifetime imaging microscope setup toward monitoring the ratio of oxidized to pristine Mito-Bodipy-TOH

based on their characteristic fluorescence lifetimes (long and short, respectively).

CONCLUSIONS

Here we have described a convergent methodology for the preparation of BODIPY-based fluorogenic antioxidants and, more generally, functionalized BODIPY dyes. Using this methodology, we have accomplished the synthesis of a 3-segment lipophilic fluorogenic antioxidant that targets the inner mitochondrial lipid membrane of live cells. Mechanistic studies in the presence of free radical sources conducted both in homogeneous and microheterogeneous systems for the new probe herein reported position its antioxidant activity on par with of α-tocopherol, the most potent naturally occurring lipid soluble antioxidant. The probe is thus characterized by a rapid rate of reaction with lipid peroxyl radicals. Both the sensitivity and the reactivity toward lipid peroxyl radicals within the inner mitochondrial membrane are unique attributes of the new probe Mito-Bodipy-TOH.

Given the location of the electron transport chain, the inner mitochondrial membrane is highly susceptible to the chemical activity of ROS. Polyunsaturated fatty acids (PUFA) within the inner mitochondrial membrane are particularly vulnerable to oxidative modifications that result in the lipid chain peroxidation. Here we have shown via a suite of imaging studies conducted on live cells that Mito-Bodipy-TOH enables real-time monitoring of lipid peroxyl radical generation and antioxidant depletion within the inner mitochondrial membrane. Our findings underscore the potential of the fluorogenic antioxidant Mito-Bodipy-TOH to investigate the relationship between antioxidant load, onset of the lipid chain autoxidation and mitochondrial physiology and mithochondrial dysfunction.

EXPERIMENTAL SECTION

Abbreviations. 2,2′-Azobis-(2-methylpropionamidine) dihydrochloride (ABAP); 2, 2′-azobis-(2-methylbutyronitrile) (AMBN); 2,2′-azobis(4-methoxy-2.4-dimethyl valeronitrile) (MeO-AMVN); benzoyl group (Bz); boron-dipyrromethene (4,4-difluoro-4-bora-3a,4a-diaza-*s*-indacene) (BODIPY); *tert*-butyloxycarbonyl group (Boc); dimethylformamide (DMF); dimethyl sulfoxide (DMSO); Dulbecco's Modified Eagle Medium (DMEM); fetal bovine serum (FBS); 4-(2-hydroxyethyl)-1-piperazineethanesulfonic acid (HEPES); L-α-phosphocholine (EggPC); methoxymethyl group (MOM); *N*,*N*′-dimethyl-4,4′-bipyridinium dichloride (Methyl Viologen) (MV^{2+}); 2,2,5,7,8-pentamethyl-6-chromanol (PMHC); α-tocopherol (TOH).

Materials. 2,2′-Azobis(4-methoxy-2.4-dimethyl valeronitrile) (MeO-AMVN) and 2,2′-azobis(2-methylbutyronitrile) (AMBN) were supplied by Wako Pure Chemical Industries, Ltd. L-α-Phosphocholine (EggPC) was obtained from Avanti Polar Lipids, (Alabaster, AL). All other chemicals were purchased from Sigma-Aldrich (Oakville, Ontario, Canada) and were used without further purification. Water was purified by a Millipore Milli-Q system.

Instrumentation. Absorption and emission spectra were recorded on a Cary 5000 UV−vis-NIR and Cary Eclipse Fluorescence Spectrophotomeres, using 1 cm × 1 cm quartz cuvettes. ^{1}H NMR and ^{13}C NMR spectra were recorded on a Varian VNMRS 500 instrument at 500 and 126 MHz, respectively. ESI mass spectra were measured on a Thermo Scientific Exactive Orbitrap.

Fluorescence Quantum Yields. PM605 in acetonitrile (Φ_{st} = 0.72) was used as a standard to calculate the emission quantum yields of the new compounds (Φ_x). The absorbance at 510 nm of solutions of PM605 in acetonitrile and the dye of interest in acetonitrile at five different concentrations were recorded. Emission spectra were recorded for all solutions using excitation and emission slits of 2.5 nm upon excitation at 510 nm. Relative quantum efficiencies with respect to the standard were obtained from the slope of the product of absorption for the standard A_{st}, integrated emission I_x and solvent refractive index n_x for the unknown Φ_x vs the product of absorption for the unknown A_x, integrated emission I_{st} and solvent refractive index n_{st} for the standard.

$$A_{st} \times I_x \times n_x^2 = \frac{\phi_x}{\phi_{st}} \times A_x \times I_{st} \times n_{st}^2$$

Steady State Fluorescence Studies. A Cary Eclipse Spectrophotometer with temperature controller was utilized to measure the emission intensity profiles of (A) 9.5 μM compounds **1** and **2** and (B) 9.0 μM α-tocopherol or PMHC solutions with 0.5 μM compounds **1** and **2** in 3 mL of acetonitrile. Fluorescence was recorded at 570 nm upon exciting at 510 nm using 2.5 nm excitation and 2.5 (for case A) or 5 nm (for case B) emission slits. A total of 2.875 mL of acetonitrile solutions containing compounds **1** or **2** with or without α-tocopherol or PMHC was incubated for 10 min at 37 °C before 125 μL of AMBN 2.028 M in acetonitrile was added to each cuvette for final AMBN concentration of 84.5 mM. The emission intensity was followed at 2.5 s intervals for 4000 s.

Liposome Preparation and Microplate Assays. Assays were conducted following a previously reported procedure.[29]

Cell Preparation and Staining. NIH 3T3 mouse embryo fibroblast cells were cultured in Dulbecco's Modified Eagle Medium (DMEM) containing high glucose with L-glutamine, phenol red, and sodium pyruvate (Gibco), supplemented with 10% fetal bovine serum (FBS) and 1% penicillin-streptomycin. Cells were maintained at 37 °C (5% CO_2) in a humidified atmosphere. Cells were trypsinized and split 1/40 once a week when confluence of cells was reached. For fluorescence microscopy, cells were passed, split 1/5, plated on 35 mm glass imaging dish (World Precision Instruments, Inc.) coated with fibronectin (1 μg/mL), and cultured in DMEM containing growth factors 1 day prior to imaging. For all experiments, solutions of dyes were prepared as follows: 60 μM MitoTracker Deep Red (Molecular Probes) or 300 μM of **2**, **3**, and **4** stock solutions in DMSO were prepared. Ten microliters of each stock solution was added to 3 mL of Dulbecco's Modified Eagle Medium (DMEM) containing high glucose with L-glutamine, without phenol red, sodium pyruvate (Gibco), or HEPES. Cells were incubated with the DMEM solutions with final concentrations of 200 nM MitoTracker Deep Red and 1 μM of either **2**, **3**, or **4** for 5 min at 37 °C (5% CO_2) in a humidified atmosphere. Following incubation, the DMEM solutions were removed and exchanged with DMEM containing high glucose, L-glutamine, and 10% fetal bovine serum (FBS), without phenol red, or sodium pyruvate.

Cells Treated with Methyl Viologen. NIH 3T3 mouse embryo fibroblast cells were prepared as described above. The DMEM growth media was removed 4 h prior to imaging and substituted with 1.5 mL of DMEM containing 1 mM MV^{2+} (methyl viologen) and glucose with L-glutamine, without phenol red, sodium pyruvate (Gibco), or HEPES. After 4 h, the MV^{2+} solution was removed, cells were washed with Dulbecco's Phosphate-Buffered Saline (DPBS) and stained as described above, and the media was exchanged to DMEM containing high glucose with L-glutamine, without phenol red, sodium pyruvate (Gibco), or HEPES.

Fluorescence Imaging Experiments. Confocal fluorescence imaging studies were performed using a Zeiss LSM 710 laser scanning microscope equipped with either a C-Apochromat 40×/1.20 W Korr M27 water-immersion objective lens or a Plan-Apochromat 100×/1.40 oil-immersion objective lens. Cells stained with either dyes **2**, **3**, or **4** and MitoTracker Deep Red were excited with the 488 nm (125 μW) laser output of a cw Ar^+ laser (for imaging **2**, **3**, or **4**) and with the 633 nm (160 μW) laser output of a cw HeNe laser (MitoTracker Deep Red). An MBS 488/543/633 dichrioc beam splitter was utilized. Emission was collected using a META detector between 500 and 620 nm and 650−740 nm, respectively, using sequential scans.

Calculations for cell fluorescence. All quantifications were performed using ImageJ software following a protocol previously published.[64,65] We used the equation below to calculate the corrected total cell fluorescence (CTCF):

$$\text{CTCF} = \text{IntDensity} - (\text{Cell Area} \times \text{BkgFluorescence})$$

where IntDensity is the integrated intensity of the pixels for one cell, Cell Area is the number of pixels in the same cell, and BkgFluorescence is the average signal per pixel for a region with no cells.

Calculations for Manders' Colocalization Coefficients. The Manders' colocalization coefficients M1 and M2 were calculated according to Manders method,[55] using the JACoP plug-in in ImageJ software. The colocalization coefficients M1 and M2 are defined by the following equations:

$$\text{M1} = \frac{\sum_i R_{i,\text{coloc}}}{\sum_i R_i} \text{ and M2} = \frac{\sum_i G_{i,\text{coloc}}}{\sum_i G_i}$$

i.e., M1 is the sum of the intensities of red pixels that have a green component divided by the total sum of red intensities and M2 is the sum of the intensities of green pixels that have a red component divided by the total sum of green intensities. M1 and M2 colocalization coefficients can be determined even when the signal intensities in the two components differ strongly as is the case with Mito-Bodipy-TOH and MitoTracker Deep Red. The intensity thresholds for each channel were determined using the Costes method.[66]

■ ASSOCIATED CONTENT

Supporting Information

Kinetic studies in homogeneous and microheterogeneous media, synthesis, IR, ^{1}H NMR and ^{13}C NMR spectra for all new compounds and precursors. This material is available free of charge via the Internet at http://pubs.acs.org.

■ AUTHOR INFORMATION

Corresponding Author

gonzalo.cosa@mcgill.ca

Notes

The authors declare no competing financial interest.

■ ACKNOWLEDGMENTS

G.C. is grateful to the Natural Sciences and Engineering Research Council (NSERC) and Canadian Foundation for Innovation (CFI) for funding. K.K. is thankful to the Drug Discovery and Training Program (CIHR) for postgraduate scholarships; L.E.G. is thankful to Vanier Canada for a postgraduate scholarship. We are also grateful to Prof. Siegfried Hekimi and Ms. Ying Cheng at McGill Biology for the use of their facilities. Imaging and image processing/analysis for this manuscript were performed in the McGill University Life Sciences Complex Imaging Facility.

■ REFERENCES

(1) Barnham, K. J.; Masters, C. L.; Bush, A. I. *Nat. Rev. Drug Discov.ery* **2004**, *3*, 205.
(2) Burton, G. W.; Ingold, K. U. *Acc. Chem. Res.* **1986**, *19*, 194.
(3) Porter, N. A. *Acc. Chem. Res.* **1986**, *19*, 262.
(4) Yin, H.; Xu, L.; Porter, N. A. *Chem. Rev.* **2011**, *111*, 5944.
(5) α-Tocopherol effectively scavenges peroxyl radicals preventing chain reactions from taking place. In its presence the kinetic chain length is 1 unless the lipids to antioxidant mole ratio is larger than 1×10^5.
(6) Finkel, T.; Holbrook, N. J. *Nature* **2000**, *408*, 239.
(7) Turrens, J. F. *J. Physiol.* **2003**, *552*, 335.
(8) Murphy, M. P. *Biochem. J.* **2009**, *417*, 1.
(9) Green, D. R.; Kroemer, G. *Science* **2004**, *305*, 626.
(10) Beal, M. F. *Ann. Neurol.* **2005**, *58*, 495.
(11) Green, D. R.; Reed, J. C. *Science* **1998**, *281*, 1309.
(12) Abou-Sleiman, P. M.; Muqit, M. M. K.; Wood, N. W. *Nat. Rev. Neurosci.* **2006**, *7*, 207.
(13) Schapira, A. H. V. *Lancet Neurol.* **2008**, *7*, 97.
(14) Guzman, J. N.; Sanchez-Padilla, J.; Wokosin, D.; Kondapalli, J.; Ilijic, E.; Schumacker, P. T.; Surmeier, D. J. *Nature* **2010**, *468*, 696.
(15) Mattson, M. P.; Magnus, T. *Nat. Rev. Neurosci.* **2006**, *7*, 278.
(16) Manfredi, G.; Xu, Z. *Mitochondrion* **2005**, *5*, 77.
(17) Girard, M.; Larivière, R.; Parfitt, D. A.; Deane, E. C.; Gaudet, R.; Nossova, N.; Blondeau, F.; Prenosil, G.; Vermeulen, E. G. M.; Duchen, M. R.; Richter, A.; Shoubridge, E. A.; Gehring, K.; McKinney, R. A.; Brais, B.; Chapple, J. P.; McPherson, P. S. *Proc. Natl. Acad. Sci. U.S.A.* **2012**, *109*, 1661.
(18) Dickinson, B. C.; Chang, C. J. *J. Am. Chem. Soc.* **2008**, *130*, 9638.
(19) Dickinson, B. C.; Srikun, D.; Chang, C. J. *Curr. Opin. Chem. Biol.* **2010**, *14*, 50.
(20) Robinson, K. M.; Janes, M. S.; Pehar, M.; Monette, J. S.; Ross, M. F.; Hagen, T. M.; Murphy, M. P.; Beckman, J. S. *Proc. Natl. Acad. Sci. U.S.A.* **2006**, *103*, 15038.
(21) Koide, Y.; Urano, Y.; Kenmoku, S.; Kojima, H.; Nagano, T. *J. Am. Chem. Soc.* **2007**, *129*, 10324.
(22) Liu, F.; Wu, T.; Cao, J.; Zhang, H.; Hu, M.; Sun, S.; Song, F.; Fan, J.; Wang, J.; Peng, X. *Analyst* **2013**, *138*, 775.
(23) Prime, T. A.; Forkink, M.; Logan, A.; Finichiu, P. G.; McLachlan, J.; Li Pun, P. B.; Koopman, W. J. H.; Larsen, L.; Latter, M. J.; Smith, R. A. J.; Murphy, M. P. *Free Radical Biol. Med.* **2012**, *53*, 544.
(24) Naguib, Y. M. A. *Anal. Biochem.* **1998**, *265*, 290.
(25) Krumova, K.; Oleynik, P.; Karam, P.; Cosa, G. *J. Org. Chem.* **2009**, *74*, 3641.
(26) Oleynik, P.; Ishihara, Y.; Cosa, G. *J. Am. Chem. Soc.* **2007**, *129*, 1842.
(27) Khatchadourian, A.; Krumova, K.; Boridy, S.; Ngo, A. T.; Maysinger, D.; Cosa, G. *Biochemistry* **2009**, *48*, 5658.
(28) Krumova, K.; Friedland, S.; Cosa, G. *J. Am. Chem. Soc.* **2013**, *135*, 1625.
(29) Krumova, K.; Freidland, S.; Cosa, G. *J. Am. Chem. Soc.* **2012**, *134*, 10102.
(30) Krumova, K.; Cosa, G. *J. Am. Chem. Soc.* **2010**, *132*, 17560.
(31) Liberman, E. A.; Topaly, V. P.; Tsofina, L. M.; Jasaitis, A. A.; Skulachev, V. P. *Nature* **1969**, *222*, 1076.
(32) Chen, L. B. *Annu. Rev. Cell Biol.* **1988**, *4*, 155.
(33) Grinius, L. L.; Jasaitis, A. A.; Kadziauskas, Y. P.; Liberman, E. A.; Skulachev, V. P.; Topali, V. P.; Tsofina, L. M.; Vladimirova, M. A. *Biochim. Biophys. Acta* **1970**, *216*, 1.
(34) Murphy, M. P. *Trends Biotechnol.* **1997**, *15*, 326.
(35) Murphy, M. P. *Expert Opin. Biol. Ther.* **2001**, *1*, 753.
(36) Murphy, M. P.; Smith, R. A. J. *Annu. Rev. Pharmacol. Toxicol.* **2007**, *47*, 629.
(37) Smith, R. A. J.; Porteous, C. M.; Coulter, C. V.; Murphy, M. P. *Eur. J. Biochem.* **1999**, *263*, 709.
(38) Abu-Gosh, S. E.; Kolvazon, N.; Tirosh, B.; Ringel, I.; Yavin, E. *Mol. Pharmaceutics* **2009**, *6*, 1138.
(39) Biasutto, L.; Mattarei, A.; Marotta, E.; Bradaschia, A.; Sassi, N.; Garbisa, S.; Zoratti, M.; Paradisi, C. *Bioorg. Med. Chem. Lett.* **2008**, *18*, 5594.
(40) Mukhopadhyay, A.; Weiner, H. *Adv. Drug Delivery Rev.* **2007**, *59*, 729.
(41) Dodani, S. C.; Leary, S. C.; Cobine, P. A.; Winge, D. R.; Chang, C. J. *J. Am. Chem. Soc.* **2011**, *133*, 8606.
(42) Hoye, A. T. D.; Jennifer, E.; Wipf, P.; Fink, M. P.; Kagan, V. E. *Acc. Chem. Res.* **2008**, *41*, 87.
(43) Bae, S. K.; Heo, C. H.; Choi, D. J.; Sen, D.; Joe, E.-H.; Cho, B. R.; Kim, H. M. *J. Am. Chem. Soc.* **2013**, *135*, 9915.
(44) Yang, Z.; He, Y.; Lee, J.-H.; Park, N.; Suh, M.; Chae, W.-S.; Cao, J.; Peng, X.; Jung, H.; Kang, C.; Kim, J. S. *J. Am. Chem. Soc.* **2013**, *135*, 9181.
(45) Loudet, A.; Burgess, K. *Chem. Rev.* **2007**, *107*, 4891.

(46) West, R.; Panagabko, C.; Atkinson, J. *J. Org. Chem.* **2010**, *75*, 2883.
(47) Wan, C.-W.; Burghart, A.; Chen, J.; Bergström, F.; Johansson, L. B. Å.; Wolford, M. F.; Kim, T. G.; Topp, M. R.; Hochstrasser, R. M.; Burgess, K. *Chem.—Eur. J.* **2003**, *9*, 4430.
(48) Tietze, L. F.; Kettschau, G.; Heuschert, U.; Nordmann, G. *Chem.—Eur. J.* **2001**, *7*, 368.
(49) Macor, J. E.; Forman, J. T.; Post, R. J.; Ryan, K. *Tetrahedron Lett.* **1997**, *38*, 1673.
(50) Holmes, R. T.; Lu, J.; Mwakwari, C.; Smith, K. M. *ARKIVOC* **2009**, *2010*, 5.
(51) Tu, B.; Wang, C.; Ma, J. *ChemInform* **1999**, 30.
(52) Barclay, L. R. C.; Baskin, K. A.; Dakin, K. A.; Locke, S. J.; Vinqvist, M. R. *Can. J. Chem.* **1990**, *68*, 2258.
(53) Valgimigli, L.; Ingold, K. U.; Lusztyk, J. *J. Am. Chem. Soc.* **1996**, *118*, 3545.
(54) Niki, E.; Noguchi, N. *Acc. Chem. Res.* **2003**, *37*, 45.
(55) Manders, E. M. M.; Verbeek, F. J.; Aten, J. A. *J. Microsc.* **1993**, *169*, 375.
(56) Cadenas, E. *Annu. Rev. Biochem.* **1989**, *58*, 79.
(57) Farrington, J. A.; Ebert, M.; Land, E. J.; Fletcher, K. *Biochim. Biophys. Acta* **1973**, *314*, 372.
(58) Cochemé, H. M.; Murphy, M. P. *J. Biol. Chem.* **2008**, *283*, 1786.
(59) Cochemé, H. M.; Murphy, M. P. In *Methods in Enzymology*; William, S. A., Immo, E. S., Eds.; Academic Press: New York, 2009; Vol. *456*, p 395.
(60) Li, B.; Harjani, J. R.; Cormier, N. S.; Madarati, H.; Atkinson, J.; Cosa, G.; Pratt, D. A. *J. Am. Chem. Soc.* **2013**, *135*, 1394.
(61) We recently reported that oxidation of liposome-embedded H_2B-PMHC (a related probe lacking the triphenylphosphonium cation) with lipophilic peroxyl radicals could be inhibited in a dose-dependent manner by added ascorbate, presumably due to scavenging of the probe-derived aryloxyl radical, see reference 60. A related probe (B-TOH) was shown to inhibit O_2 consumption in oxygen uptake studies upon peroxyl radical initiated styrene autoxidation, see reference 25. Both these processes are characteristic features in α-tocopherol antioxidant activity (ref 2). They support the antioxidant assignment of our family of receptor-reporter probes based on a chromanol moiety tethered to a bodipy fluorophore.
(62) Krumova, K.; Cosa, G. In *Photochemistry*; The Royal Society of Chemistry: Cambridge, U.K., 2013; Vol. *41*, p 279.
(63) Yoshida, Y.; Shimakawa, S.; Itoh, N.; Niki, E. *Free Radical Res.* **2003**, *37*, 861.
(64) Gavet, O.; Pines, J. *Dev. Cell* **2010**, *18*, 533.
(65) Burgess, A.; Vigneron, S.; Brioudes, E.; Labbé, J.-C.; Lorca, T.; Castro, A. *Proc. Natl. Acad. Sci. U.S.A.* **2010**, *107*, 12564.
(66) Costes, S. V.; Daelemans, D.; Cho, E. H.; Dobbin, Z.; Pavlakis, G.; Lockett, S. *Biophys. J.* **2004**, *86*, 3993.